A Hybrid Wireless Power Transfer System With Constant and Enhanced Current Output Against Load Variation and Coupling Misalignment

Xiaodong Qing, *Member, IEEE*, Zuojin Li, *Member, IEEE*, Xueying Wu, Zhe Liu, Lei Zhao, *Member, IEEE*, and Yugang Su, *Member, IEEE*

***Abstract*—Inductive power transfer and capacitive power transfer (CPT) are two of the most commonly used near-field wireless power transfer technologies, and these two systems share similarities and symmetries. This article proposes a hybrid wireless power transfer (HWPT) system to achieve load-independent characteristic and anti-misalignment capability. The HWPT system utilizes the compensation inductors of the CPT system to create an additional inductive channel in which the capacitive and inductive channels are compensated for each other. Based on the modeling of the HWPT system, the load-independent and enhanced constant current output is derived. In HWPT system, the inductive coupler is employed with the capacitive coupler, which forms a compact hybrid coupler. As the coupler becomes misaligned, the loss of power transferred through the inductive channel can be compensated by the increase of power transferred through the capacitive channel. A 200 W experimental prototype is built to validate the performance of the HWPT system. Experimental results show that as the load resistance ranges from 20 to 40 Ω and the coupling misalignment ranges from 0 to 100 mm, the output current remains nearly constant and the input current stays in phase with the input voltage. According to the experimental findings, the output current of the HWPT system is approximately twice as high as that of the CPT system when using the same capacitive coupler.**

***Index Terms*—Capacitive and inductive coupler, compensation inductor, capacitive power transfer (CPT), hybrid wireless power transfer (HWPT).**

I. Introduction

WIRELESS power transfer (WPT) technology utilizes the soft medium to deliver power through a relatively large air gap. Over the last decade, inductive power transfer (IPT) and capacitive power transfer (CPT) are the two most popular near-field WPT technologies [1], [2], and they are ready to be applied in many fields, such as consumer electronics [3], [4], underwater equipment [5], [6], and electric vehicle [7], [8], [9].

For both IPT and CPT systems, the power transmission ability is dependent on the coupling coefficient. However, the coupling coefficient is challenging to improve, because the size of the coupler is limited by applications. In [10], a multilayer coil is proposed for IPT systems to increase the mutual inductance. However, this structure increases system volume and cost. In [11], an interleaved capacitive coupler is proposed to obtain a larger mutual capacitance. However, the structure is complex and sensitive.

Actually, there are many similarities and dualities between the IPT and CPT systems. The inductive (capacitive) coupler and capacitive (inductive) components exist and compensate for each other in the IPT (CPT) system [12], [13]. Thus, it is possible and meaningful to combine them to form a hybrid wireless power transfer (HWPT) system to improve transmission performance [14], [15].

In some applications, a constant current (CC) output is required for WPT systems. For instance, maintaining battery charge between 20% and 80% is beneficial for battery life, and the charging process between these levels is always CC charging. However, the system output can be largely affected by the load resistance and coupling condition, where the load resistance varies during the charging process and the coupling parameters vary as the coupler misaligned. In practice, the HWPT system with both load-independent characteristic and antimisalignment ability is preferred [16], [17], [26].

Numerous approaches have been proposed to achieve a constant output, which can be broadly classified into three categories: system control, compensation network, and coupler design. For the system control, a common approach is applying a dc–dc converter to regulate the output power. However, this method brings extra losses and makes the system complex. In [18], a frequency regulation based on H_∞ is proposed for the IPT system to regulate the output power. However, the frequency regulation may cause a system stability problem, i.e., frequency bifurcation. For the compensation network, a hybrid IPT topology is also proposed for achieving a constant output [20], but the system design is complex including multiple reactive power components. A parameter design method for *LC*–*LC* compensated CPT system is proposed to achieve a nearly

Manuscript received 21 February 2023; revised 1 May 2023, 14 June 2023, and 30 June 2023; accepted 10 July 2023. Date of publication 17 July 2023; date of current version 1 September 2023. This work was supported by the Natural Science Foundation of Chongqing under Grants 2023NSCQ-MSX3764 and CSTC2021CJH-BGZM0071. Recommended for publication by Associate Editor A. Safaee. *(Corresponding authors: Lei Zhao; Zuojin Li.)*

Xiaodong Qing, Zuojin Li, and Xueying Wu are with the School of Electrical Engineering, Chongqing University of Science and Technology, Chongqing 400044, China (e-mail: 2021039@cqust.edu.cn; cqustlzj@sina.cn; 975623914@qq.com).

Zhe Liu, Lei Zhao, and Yugang Su are with the College of Automation, Chongqing University, Chongqing 400044, China (e-mail: 809632730@qq.com; lzha915@cqu.edu.cn; su7558@qq.com).

Color versions of one or more figures in this article are available at https://doi.org/10.1109/TPEL.2023.3296274.

Digital Object Identifier 10.1109/TPEL.2023.3296274

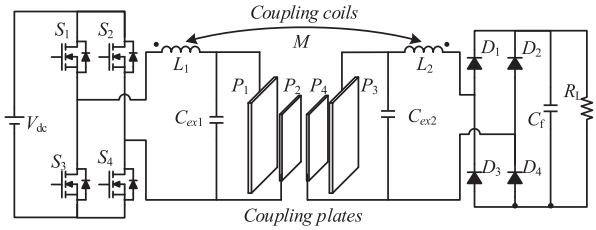

Fig. 1. Main topology of the proposed HWPT system.

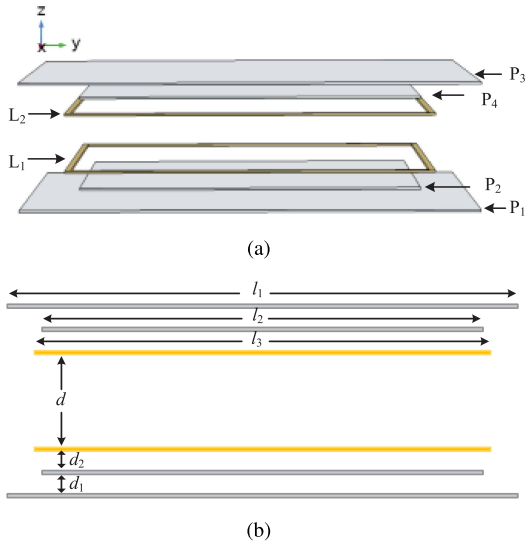

Fig. 2. Structure and dimension of the hybrid coupler. (a) 3-D view. (b) Front view.

constant output against load variation and coupling misalignment [19]. However, this system operates in the detuning state, resulting in increased reactive power, power loss, and VA rating. For the coupler design, a capacitive coupler array is proposed to overcome coupling misalignment [3]. However, using matrix plates as the transmitting end could increase electric-field radiation and reduce system efficiency. In [21], a design method for inductive coupler is proposed to improve the antioffset ability. However, the inductive coupler is heavy and expensive. In addition, an *LC–LC* compensated CPT-based HWPT system for railway applications is proposed in [15]. However, the direct connection of two outer plates of the capacitive coupler limits the system's application.

Nevertheless, how to combine IPT and CPT systems to achieve the load-independent characteristic and antimisalignment ability needs to be further studied. Driven by these motivations, this article proposes an HWPT system with a constant and enhanced current output. The main contributions of this article are summarized as follows.

1) Based on the circuit model of the HWPT system, this article reveals the working principle to achieve the load-independent CC output and zero phase angle (ZPA) by combing IPT and CPT systems.
2) The output is negatively correlated with the mutual capacitance, as well as positively correlated with the mutual inductance so that the HWPT system can achieve antimisalignment characteristic with the well-designed coupler.
3) Both the capacitive coupled and inductive coupled channels are used to transfer power leading to enhanced power transmission. Meanwhile, the inductive coupler is employed together with the capacitive coupler to form a concise structure.

The rest of this article is organized as follows. Section II introduces the system architecture of the proposed HWPT system. Based on the mathematical model, the working principle of the HWPT system is analyzed in Section III. The system design is presented in Section IV, including coupler design. Experimental prototype are carried out to validate the performance of the HWPT system in Section V. Finally, Section VI concludes this article.

II. System Architecture

A. Proposed HWTP System

In this article, the system architecture of the proposed HWPT system is shown in Fig. 1. The main circuits is composed of the dc power supply, high-frequency full-bridge inverter formed by $S_1 - S_4$, double-sided *LC* compensation network, vertical capacitive coupler, rectifier, and the load resistance R_L. C_{ex1} and C_{ex2} are placed on the primary and secondary sides to increase the self-capacitances of the capacitive coupler. As shown in Fig. 1, there is inductive coupling between the compensation inductors, where M represents the mutual inductance.

B. Hybrid Coupler

In the proposed HWPT system, the hybrid coupler is consist of a capacitive coupler and an inductive coupler. To make a concise structure, the inductive coupler is positioned between the capacitive coupler, as shown in Fig. 2. *Q*-type coils are employed as the inductive coupler, while vertical structure is selected as the capacitive coupler. For the consistency of the *X*- and *Y*-axis, the plates and coils are designed to be symmetric from the primary to the secondary side. As depicted in Fig. 2(a), P_1, P_2, and L_1 are fixed as the transmitter, while P_3, P_4, and L_2 are installed on the application as the receiver. As shown in Fig. 2(b), the length of P_1 and P_3 is l_1, the length of P_2 and P_4 is l_2, the inner diameter of coils is l_3. The transmission distance between coils is d, the distance between plates on the same side is d_1, the separated distance between plat and coil on the same side is d_2. The specific design of the hybrid coupler is presented in Section IV.

III. Working Principle

A. Modeling of Capacitive Coupler

For the capacitive coupler, there is one coupling capacitor between each two coupling plates, resulting in a six-capacitor model, as depicted in Fig. 3(a). It is a typical two-port network, which can be equivalent to a current-source model, as demonstrated in Fig. 3(b). In this model, considering the extra capacitances C_{ex1} and C_{ex2}, the self-capacitance and mutual

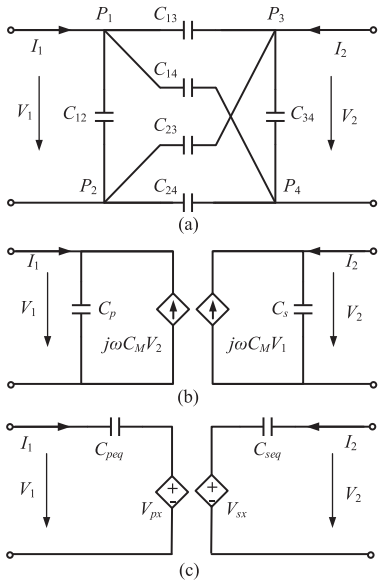

Fig. 3. Equivalent circuit of the capacitive coupler. (a) Six-capacitances circuit. (b) Current source model. (c) Voltage source model.

capacitance can be given as

$$\begin{cases} C_p = C_{\text{ex1}} + C_{12} + \dfrac{(C_{13}+C_{14})(C_{23}+C_{24})}{C_{13}+C_{14}+C_{23}+C_{24}} \\ C_s = C_{\text{ex2}} + C_{34} + \dfrac{(C_{13}+C_{24})(C_{14}+C_{24})}{C_{13}+C_{14}+C_{23}+C_{24}} \\ C_M = \dfrac{C_{13}C_{24} - C_{14}C_{23}}{C_{13}+C_{14}+C_{23}+C_{24}} \end{cases} \tag{1}$$

where, C_{ij} represents the coupling capacitance between P_i and P_j. Similar to the coils, the capacitive coupling coefficient is defined as k_c, which can be expressed as

$$k_c = C_M / \sqrt{C_p C_s}. \tag{2}$$

For the HWPT system, due to the inductive channel between the compensation inductors, a series compensation topology of the capacitive coupler is more suitable for the circuit analysis. Therefore, the current source model can be converted to the voltage source model, as shown in Fig. 3(c). According to the equivalent circuit, the equivalent capacitance and voltage sources in Fig. 3(c) can be expressed as

$$\begin{cases} C_{\text{peq}} = \dfrac{C_p C_s - C_M^2}{C_s} \\ C_{\text{seq}} = \dfrac{C_p C_s - C_M^2}{C_p} \\ C_{\text{Meq}} = \dfrac{C_p C_s - C_M^2}{C_M} \end{cases} \tag{3}$$

$$\begin{cases} V_{px} = \dfrac{C_M}{j\omega\left(C_p C_s - C_M^2\right)} \cdot I_2 \\ V_{sx} = \dfrac{C_M}{j\omega\left(C_p C_s - C_M^2\right)} \cdot I_1. \end{cases} \tag{4}$$

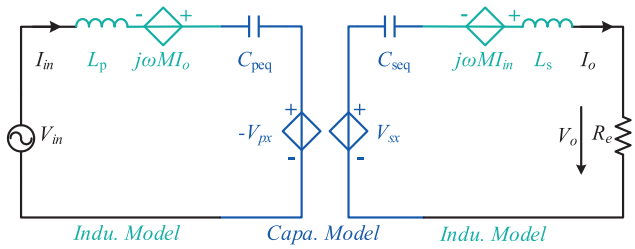

Fig. 4. Equivalent circuit of the proposed HWPT system under the fundamental component.

B. CC Output Against Load Variation

Due to good filtering function of compensation network, the current in primary side is nearly sinusoidal containing only fundamental component. Based on the fact that only the fundamental component of the voltage source on ac-side contributes to power transfer, the fundamental harmonic approximation (FHA) method is adopted in this article. Based on the voltage source models of the capacitive and inductive couplers, the equivalent circuit of the proposed HWPT system is shown in Fig. 4. It is a typical SS compensation circuit, yet it contains four controlled voltage sources. Two voltage sources $j\omega M I_{\text{in}}$ and $j\omega M I_o$ represent the inductive coupling. Two voltage sources V_{px} and V_{sx} represent the capacitive coupling. R_e indicates the equivalent resistance, $R_e = 8R_L/\pi^2$. V_{in} indicates the fundamental component of the inverter's output voltage.

In the double-sided *LC* CPT system [17], the self-resonant frequencies ω_1 and ω_2 are defined as the tuned frequency of the primary and secondary sides. If the self-resonant frequencies are designed to be the same, the following equation can be obtained:

$$\begin{cases} \omega_1^2 L_p C_p = \omega_2^2 L_s C_s = 1 \\ \omega_1 = \omega_2 = \omega_0. \end{cases} \tag{5}$$

Actually, when the primary and secondary compensation networks are fully tuned at the switching frequency ω in Fig. 4, the system output is determined by the controlled sources. Combing (3), the parameters satisfy

$$\begin{cases} \omega^2 L_p C_{\text{peq}} = \omega^2 L_p \cdot \frac{C_p C_s - C_M^2}{C_s} = \omega^2 L_p C_p \left(1 - k_c^2\right) = 1 \\ \omega^2 L_s C_{\text{seq}} = \omega^2 L_s \cdot \frac{C_p C_s - C_M^2}{C_p} = \omega^2 L_s C_s \left(1 - k_c^2\right) = 1. \end{cases} \tag{6}$$

Therefore, the frequency ω_{cc} can be expressed by ω_0

$$\omega_{\text{cc}} = \omega_0 / \sqrt{1 - k_c^2}. \tag{7}$$

According to the KVL, the input and output of the HWPT system can be expressed as

$$\begin{cases} V_{\text{in}} = -j\omega_{\text{cc}} M I_o - \dfrac{C_M}{j\omega_{\text{cc}}\left(C_p C_s - C_M^2\right)} \cdot I_o \\ V_o = j\omega_{\text{cc}} M I_{\text{in}} + \dfrac{C_M}{j\omega_{\text{cc}}\left(C_p C_s - C_M^2\right)} \cdot I_{\text{in}} = R_e I_o. \end{cases} \tag{8}$$

TABLE I
SYSTEM PARAMETERS

Parameter	Value	Parameter	Value
f_0/MHz	1.0	C_M/pF	12.2
$L_{11}(L_{21})/\mu$H	89.3	M/μH	2.5
$L_{12}(L_{22})/\mu$H	12.0	$C_p(C_s)$/pF	250.0

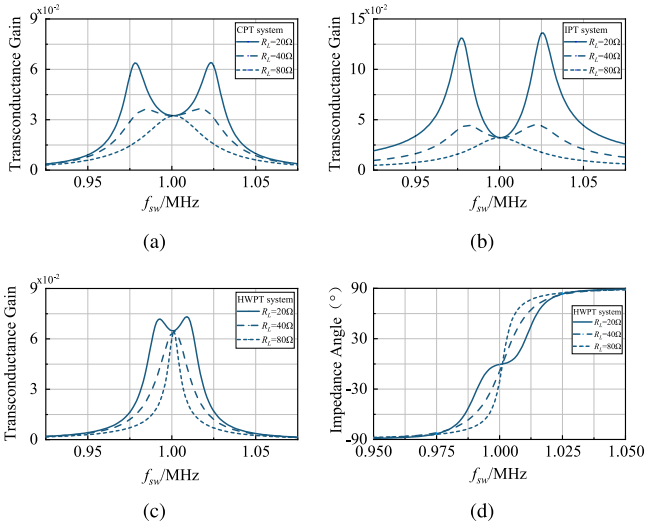

Fig. 5. Frequency properties. (a) Transconductance gain of CPT system. (b) Transconductance gain of IPT system. (c) Transconductance gain of HWPT system. (d) Impedance angle of HWPT system.

According to (5)–(8), the input current and output current can be calculated and simplified as

$$\begin{cases} I_o = -\dfrac{j\omega_0\sqrt{C_1C_2}\sqrt{1-k_c^2}}{k_c - M\omega_0^2\sqrt{C_1C_2}} \cdot V_{\text{in}} \\ I_{\text{in}} = \dfrac{\omega_0^2 C_1 C_2 \left(1-k_c^2\right) R_e}{\left(k_c - M\omega_0^2\sqrt{C_1C_2}\right)^2} \cdot V_{\text{in}}. \end{cases} \tag{9}$$

It can be seen from (9) that the output current is load-independent, which is determined by inherent parameters, i.e., C_1, C_2, ω_0, k_c, M, and V_{in}. Compared with the CPT system, the output current of the HWPT system is additionally affected by the mutual inductance. As long as $k_c > M\omega_0^2\sqrt{C_1C_2}$, the output current of the HWPT system is larger than that of the CPT system. Therefore, the output current can be increased by adjusting the mutual inductance.

C. Frequency Properties

Considering the full tuned state, the input impedance of the proposed HWPT system can be expressed as

$$Z_{\text{in-hwpt}} = \frac{\omega_0^2 C_1 C_2 (1-k_c^2) R_e}{(k_c - M\omega_0^2\sqrt{C_1C_2})^2}. \tag{10}$$

As given in (10), the impedance of proposed HWPT systems is pure resistive, which implies that ZPA can be achieved at different load resistances.

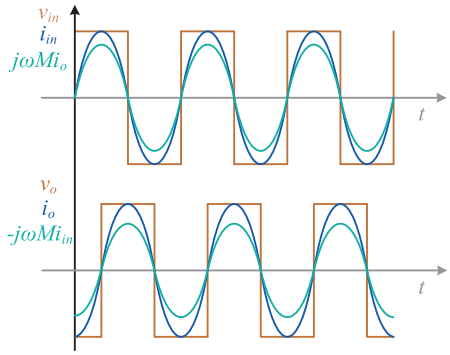

Fig. 6. Typical waveforms of the proposed HWPT system.

With the parameters listed in Table I, Fig. 5(c) and (d) shows the frequency properties of the HWPT system. With the same coupling coefficient, Fig. 5(a) and (b) shows the transconductance gain of the CPT and IPT systems, respectively. It can be seen that there is a CC frequency ω_{cc} in CPT, IPT, and HWPT systems. It also shows that the output current of the HWPT system is twice as big as that of other systems. As shown in Fig. 5(d), when the HWPT system is operated at the CC frequency, the impedance angle keeps 0° against load variation.

According to the abovementioned analysis, Fig. 6 shows the typical waveform of the HWPT system. It can be seen that the input current $\boldsymbol{i_{\text{in}}}$ is in phase with the input voltage $\boldsymbol{v_{\text{in}}}$, as well as ahead of the output current $\boldsymbol{v_o}$ by 90°, which is consistent with the *LC–LC* compensated CPT system. In addition, the induced voltages $\boldsymbol{j\omega M i_{\text{in}}}$ and $\boldsymbol{j\omega M i_o}$ are in phase or antiphase to the output and input voltage, respectively. It indicates that the additional inductive channel only changes the amplitude instead of its phase. The induced voltage $\boldsymbol{j\omega M i_{\text{in}}}$ on the secondary side is proportional to the load resistance according to (10), so that the output current of the proposed HWPT system can still remain load-independent.

Obviously, the proposed HWPT system in this article can be seen as the series connection of an IPT system and a CPT system. If there is no coupling between the compensation inductors, this system is an isolated CPT system with *LC–LC* compensation network. If there is no capacitive coupling, this system is an IPT system with SS topology.

D. CC Output Against Coupling Misalignment

In the HWPT system, the output current is negatively correlated with k_c, while it is positively correlated with M. Typically, both k_c and M decrease with the increasing coupling misalignment. It is possible to achieve a CC output against coupling misalignment with a well-designed coupler.

For a loosely coupled capacitive coupler, the mutual capacitance is determined by the cross capacitance between the primary and secondary plates, and the self-capacitance is mainly determined by the coupling capacitance of plates on the same side. Therefore, the mutual capacitance decreases with increasing coupling misalignment, while the coupling misalignment has little effect on the self-capacitance. Thus, the self-resonant

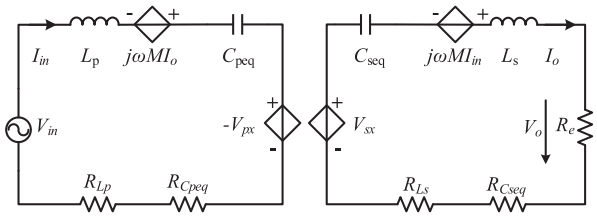

Fig. 7. Equivalent circuit with parasitic resistances.

frequency of the system can be considered to be constant. Since the capacitive coefficient is always at a very small level, the CC frequency ω_{cc} ($\omega_{cc} = \omega_0/\sqrt{1-k_c^2}$) of the HWTP system can be approximately regarded as consistent.

According to (9), the output current under coupling misalignment is set equal to the target value, the corresponding mutual inductance M can be obtained

$$M - M_{\text{mis}} = \frac{k_c - k_{c\_\text{mis}}}{\omega_0^2\sqrt{C_1 C_2}} \tag{11}$$

where, k_{c_mis} and M_{mis} represent the capacitive coefficient and mutual inductance of the coupler with coupling misalignment, respectively.

E. System Efficiency

In previous literatures [22], [23], the equivalent model with parasitic resistances of the WPT system have be analyzed. The parasitic resistance of inductor and capacitor can be expressed as equivalent series resistance. Fig. 7 shows the equivalent circuit, where the parasitic resistances are defined as R_{Lp}, $R_{C\text{peq}}$, $R_{C\text{seq}}$, and R_{Ls}. In this article, the he quality factors of L_p and L_s is defined as Q_L, and the quality factors of C_{peq} and C_{seq} is defined as Q_C

$$Q_L = \frac{\omega L_p}{R_{Lp}} =, Q_C = \frac{1}{\omega C_{\text{peq}}\, R_{\text{Cpeq}}}. \tag{12}$$

From Fig. 7, the system efficiency can be expressed as

$$\begin{aligned}\eta &= \frac{I_o^2 R_e}{I_{\text{in}}^2 R_p + I_o^2 R_s + I_o^2 R_e} \\ &= \frac{1}{R_e + R_s + \frac{(R_e+R_s+X_s)^2}{\left(\omega M - \frac{1}{\omega C_{\text{Meq}}}\right)^2} R_p}\end{aligned} \tag{13}$$

where, R_p is the sum of R_{Lp} and $R_{C\text{peq}}$. R_s is the sum of R_{Ls} and $R_{C\text{seq}}$. X_s indicates the imaginary part of the impedance on the secondary side.

According to (14), it can be noted that the efficiency is maximized by taking $\partial\eta/\partial Re = 0$, so that the maximum efficiency η_{max} and normalized load R_{base} are expressed as

$$\begin{cases} R_{\text{base}} = R_s\sqrt{1 + \frac{\left(\omega M - \frac{1}{\omega C_{\text{Meq}}}\right)^2}{R_p R_s}} \\ \eta_{\text{max}} = 1 - \frac{2}{\sqrt{1 + \frac{\left(\omega M - \frac{1}{\omega C_{\text{Meq}}}\right)^2}{R_p R_s}} + 1}. \end{cases} \tag{14}$$

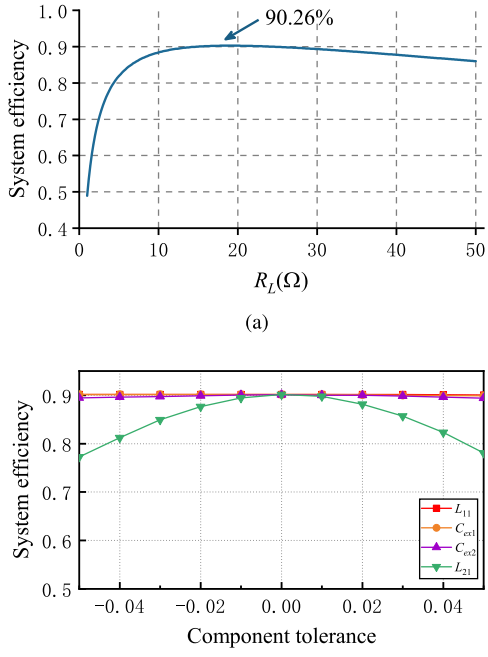

Fig. 8. System efficiency versus (a) load resistance and (b) component tolerance.

In [24], the quality factors of inductors and capacitors at different frequency are given. In this section, Q_L and Q_C are selected as 750 and 3000 according to [24], when the switching frequency is about 1 MHz. With the parameters listed in Table I, the system efficiency (ignoring losses of inverter and rectifier) is shown in Fig. 8(a). It can be seen that when the load resistance is 19.4 Ω, the system efficiency reaches the maximum value 90.26%. Since L_{12}, L_{22}, C_{ij}, and C_M are determined by the hybrid coupler, Fig. 8(b) shows the efficiency versus component tolerance. It can be seen that L_{11}, C_{ex1}, and C_{ex2} have little effect on the system efficiency within 5% error. By comparison, the system efficiency decreases about 2.5% when the error of L_{21} is ±2%.

F. Harmonics Analysis

As previous analysis, the FHA method is adopted in this article, which ignores the high-order harmonics. Actually, the output voltage of the inverter is a typical square wave, so it is necessary to analyze the influence of high-order harmonics on the power transmission. The output voltage of the inverter can be expanded according to Taylor series

$$v(t) = \frac{4V_{\text{dc}}}{\pi}\left(\sin\omega t + \frac{1}{3}\sin 3\omega t + \cdots + \frac{1}{n}\sin n\omega t + \cdots\right) \tag{15}$$

where, $n = 2k+1$, k represents positive integer.

According to the superposition theorem, the system performance under different harmonicas can be determined individually. If the network is excited by the nth harmonica, the equivalent circuit can be also simplified as the voltage coerce

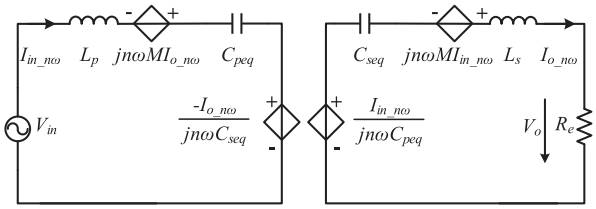

Fig. 9. Equivalent circuit of the proposed HWPT system under the nth harmonic.

models, as shown in Fig. 9. It should be point out that all induced voltage sources is excited by the frequency $n\omega$ and the equivalent inductors and capacitors remain unchanged.

According to KVL, the input and output of the HWPT system under nth harmonic can be expressed as

$$\begin{cases} V_{\text{in\_}n\omega} = (X_{Lp} + X_{C\text{peq}})I_{\text{in\_}n\omega} - (X_M + X_{\text{Meq}})I_{o\_n\omega} \\ R_e I_{o\_n\omega} = (X_M + X_{\text{Meq}})I_{\text{in\_}n\omega} - (X_{Ls} + X_{C\text{seq}})I_{o\_n\omega} \end{cases} \tag{16}$$

where, X represents the impedance.

According to Section III-B, the parameters on the primary side and secondary are designed equal, and the primary and secondary compensation networks are fully tuned at the switching frequency ω. Therefore, the input current $I_{\text{in\_}n\omega}$ and output current $I_{o\_n\omega}$ can be expressed

$$\begin{cases} I_{\text{in\_}n\omega} = \dfrac{V_{\text{in\_}n\omega}(n^2R_e + jn\omega L_p(n^2-1))}{jn\omega L_p R_e(n^2-1) - \omega^2 L_p^2(n^2-1) + (\frac{1}{\omega C_{\text{Meq}}} - n^2\omega M)^2} \\ I_{o\_n\omega} = \dfrac{V_{\text{in\_}n\omega}(\frac{1}{j\omega C_{\text{Meq}}} - jn^2\omega M)}{jn\omega L_p R_e(n^2-1) - \omega^2 L_p^2(n^2-1) + (\frac{1}{\omega C_{\text{Meq}}} - n^2\omega M)^2}. \end{cases} \tag{17}$$

With the parameters listed in Table I, the normalized input current and output current under different harmonics are shown in Fig. 10(a). As shown, the normalized input current and output current under high-order harmonics is close to zero, which is far less than those under fundamental harmonics. Therefore, the contribution of high-order harmonics to the power transmission is very small. In addition, the total harmonic distortion (THD) characterizes the circuit's ability to suppress high-order harmonics. The smaller the THD is, the stronger the suppression ability is. With the parameters listed in Table I, the THD at different inductance L_p and load resistance R_L is shown in Fig. 10(b). It can be seen that the THD of the proposed HWPT system is relatively low. The THD is positively correlated with the inductances, while it is negatively correlated with the load resistances. Therefore, the higher the quality factor of the compensation network is, the better the harmonic suppression ability is.

In summary, the high-order harmonic have little effect on the power transmission, which means the compensation network of the proposed HWPT system shows good filtering characteristic. Therefore, the FHA method can be adopted in this article to analyze the working principle.

IV. System Design and Simulation

A. Parameter Design

The whole design process is depicted as Fig. 11, where the coupler design process is shown in the dashed box. In practice,

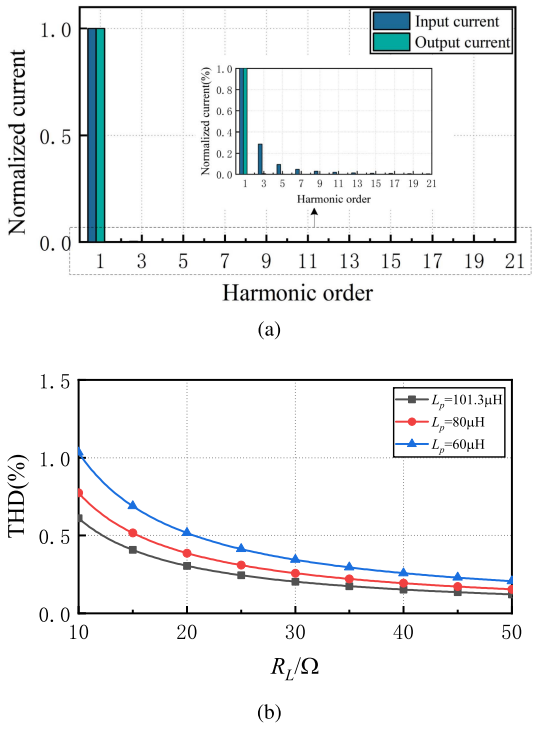

Fig. 10. (a) Normalized input current and output current under different harmonics. (b) THD versus load resistance at different inductances.

the load and output current/power are given according to the application and requirement. Usually, the working frequency of the inductive channel is several tens kHz, while that of the capacitive channel is several hundred kHz to several MHz. Considering the power transmission in both channels, the switching frequency is chosen around 1 MHz.

Actually, the volume of the hybrid coupler is limited by the application, so that the maximum size and transmission distance can be determined. Through coupler design, the coupling parameters of the hybrid coupler can be obtained. C_{ex1} and C_{ex2} are used to adjust the self-capacitances and capacitive coefficient for achieving the desired output current. Detailed design method of the hybrid coupler can be found in the next section.

According to (6), the total inductance L_p and L_s can be determined. In the HWPT system, the compensation inductance can be divided into two parts. The self-mutual is determined by the coupler, so that the inductance L_{12} and L_{22} can be calculated. Usually, a large inductance would lead to excessive winding losses and make the system bulky. The resonant inductance should satisfy

$$L_{\text{design}} \leq L_{\max} \tag{18}$$

where, $L_{\max}$ depends on the dimensional requirement and efficiency requirement of the system. If the designed inductance is larger than $L_{\max}$, the design procedure reruns with adjusting the extracapacitance, switching frequency, or input voltage.

B. Coupler Design

As described earlier, the coupling parameters of the hybrid coupler are directly related to the system performance, so that

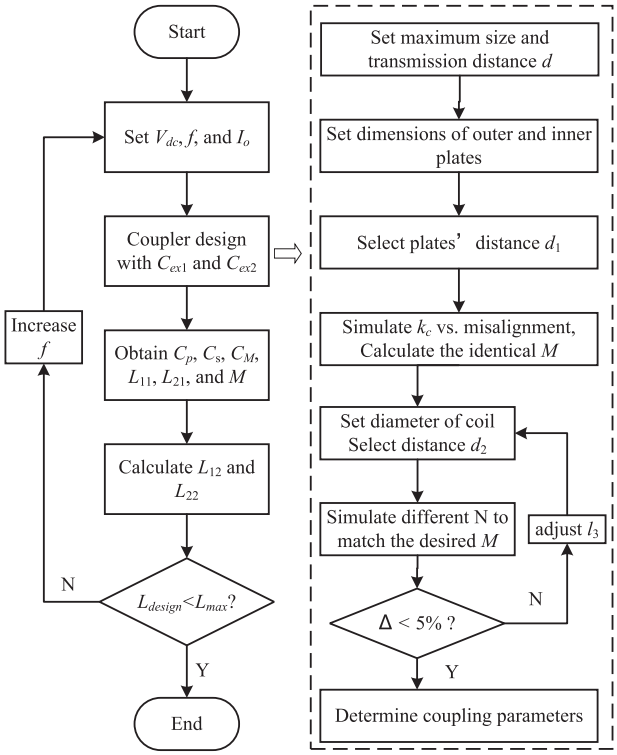

Fig. 11. Design process of the proposed HWPT system.

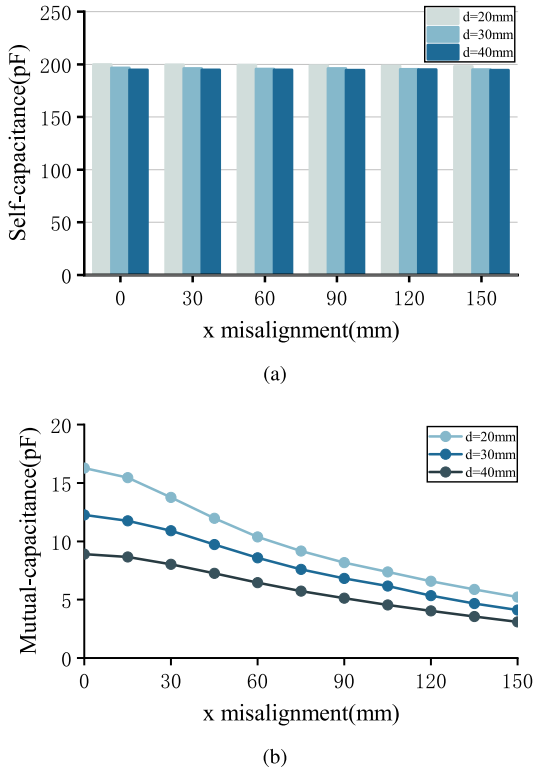

Fig. 12. Simulation results of (a) self-capacitances and (b) mutual capacitances against the coupling misalignment.

TABLE II
DIMENSIONS AND MATERIALS OF THE HYBRID COUPLER

Channel	Material	Resistivity($\Omega.m$)	Label	Size(mm)
Capacitive	Aluminum	$2.83 * 10^{-8}$	l_1	400
			l_2	300
			d_1	5
Inductive	Copper	$1.75 * 10^{-8}$	l_3	320
			d	20
			d_2	5

the well-design coupler is significant for the HWPT system. According to Section III, the anti-misalignment ability depends on the coupling parameters. Therefore, the hybrid couple is designed to achieve the antimisalignment ability. According to system architecture, it utilizes the compensation inductors of the CPT system to create an additional inductive channel, and the inductive channel is used to compensate the capacitive channel. Therefore, the capacitive coupler is designed first, and then the inductive coupler is designed based on this. The structures and dimensions of the hybrid coupler are shown in Fig. 2, where both the primary side and secondary side have the same plate and coil structures. As depicted in Fig. 11, the design process of the hybrid coupler is shown in the dashed box. Table II lists the dimensions and materials of the hybrid coupler.

For the vertical coupler, the mutual capacitance is determined by the cross capacitance between the primary and secondary plates, and the self-capacitance is mainly determined by the coupling capacitance of plates on the same side. Aluminum is a good conductor, and it shows the advantages of cheap, good plasticity, and easy to obtain. Therefore, aluminum plates are selected as the coupling plates of capacitive coupler. Considering the space limitation, the dimension of the outer plate is selected as 400 mm × 400 mm, which is listed in Table II. According to [29], the area of inner plate is designed about half of that of outer plate to achieve high coupling capacitance. Therefore, the inner plate is selected as 300 mm × 300 mm. The thickness of all plates is 1 mm. In general, the mutual capacitance and self-capacitance are negatively correlated with the plates distance d_1. However, a larger d_1 means a larger coupler volume. Therefore, the plates distance d_1 is selected as 5 mm.

The variations of self-capacitance and mutual capacitance with coupling misalignments at different coupling distances are shown in Fig. 12. Since the coupler is symmetric, two self-capacitances are always equal under different coupling misalignments. It can be seen from Fig. 12 that the transmission distance and coupling misalignment have little effect on the self-capacitance. The mutual capacitance decreases with the increment of transmission distance and coupling misalignment.

According to the theoretical analysis in Section III, the compensation inductance can be divided into two parts, $L_{12}(L_{22})$ is only used to compensate capacitance, $L_{11}(L_{21})$ the other is used to compensate the capacitive reactance and also to form the inductive channel. Thanks to the structure of the HWPT system, if the total inductance is expected, the self-inductance of the inductive coupler does not affect the output current. As depict in (11), the goal is to design the inductive coupler for achieving the identical mutual inductances, which can achieve the antimisalignment ability.

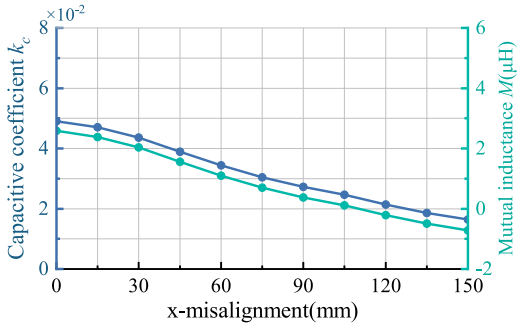

Fig. 13. Variation of k_c and corresponding M with coupling misalignment.

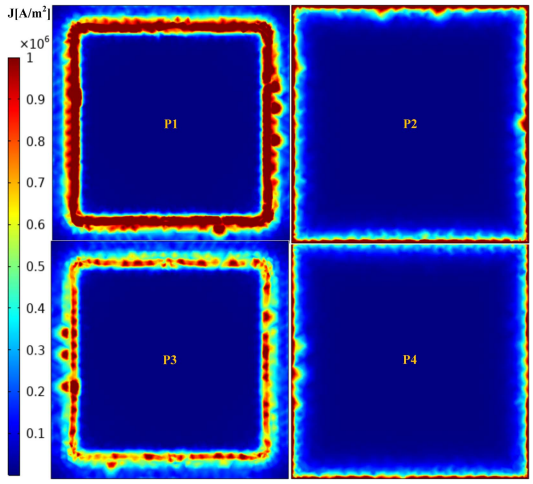

Fig. 14. Eddy current density of the coupling plates in *XY* view.

As we know, the mutual inductance of the coupler is determined by the geometry, size, air distance, and turns of the coils. Since the dimensions and distance of the coils are fixed, it is necessary to achieve the desired mutual inductance M by changing the turns of coils. To reduce the opposing area between plates and coils, the inner diameter of coils is slightly larger than that of inner plates, and the outer diameter should be smaller than that of outer plates. Therefore, the inner diameter is selected as 320 mm. In practice, the transmission distance is determined by the application. In this article, the air gap d is chosen to be 20 mm. As discussed in the next section, the large d_2 could reduce the eddy current loss, but it would increase the coupler's volume. In similar, the distance d_2 between plate and coil is selected as 5 mm.

With the parameters listed in Table II, Fig. 13 shows the variation of capacitive coefficient with coupling misalignment. To keep the output current constant under coupling misalignment, the variation of theoretical mutual inductance M is also shown in Fig. 13. It is an effective method to match the ideal mutual inductance by adjusting the number of coil turns. If M is difficult to meet the identical mutual inductance, it is better to slightly increase l_3 to reset the turns of coils.

According to (9) and (11), the inductive channel is used to enhance the output current and achieve the antimisalignment ability. It can be found that once the required output current is determined, the maximum acceptable value of coupling misalignment can also be obtained. If the coupling misalignment in application is larger than the maximum value, the HWPT system cannot ensure the CC output at this situation.

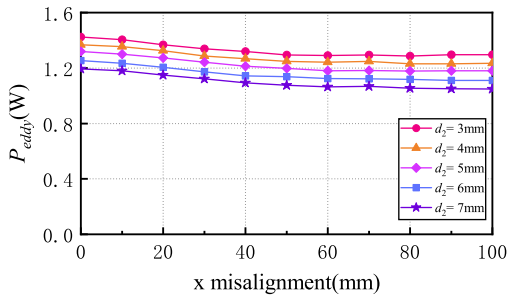

(a)

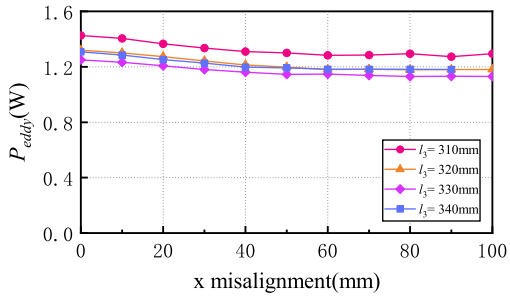

(b)

Fig. 15. Eddy current loss of the coupler versus x-misalignment under (a) different d_2 and (b) different l_3.

C. Eddy Current Loss

Under a time varying magnetic field, the eddy current is induced in the coupling plates, while H_i induced by the eddy current will oppose the source field. In general, the eddy current loss can be calculated by

$$P_{\text{eddy}} = \rho \int_V J^2 dV \tag{19}$$

where, ρ represents the resistivity, J represents the eddy current density.

Fig. 14 shows the eddy current density of plates P_1, P_2, P_3, and P_4. Since the plates and coils are rectangle, the eddy currents of plates are all centrosymmetric. Due to the structure and size of the coupler, the eddy current of P_1 induced by the excitation source reaches maximum value, while the eddy current of P_4 reaches minimum value.

The eddy current loss of the coupler versus x-misalignment at different d_2 and l_3 is shown in Fig. 15. It can be seen from Fig. 15(a) that the eddy current loss of the coupler slightly decreases with the increase of x-misalignment and separated distance d_2. There are two reasons for this: 1). the eddy current loss induced by the coil on the same side is the main part, and it keeps nearly constant with the increasing x-misalignment. 2). the eddy current loss induced by the coil on the other side decreases

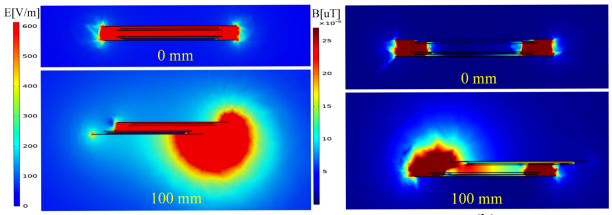

Fig. 16. Simulation results of the compact coupler at different x-misalignment. (a) Electric field. (b) Magnetic flux.

TABLE III
EXPERIMENTAL PARAMETERS

Parameter	Value	Parameter	Value
$V_{\rm dc}$/V	50	f_0/MHz	1.0
M/μH	2.4	C_M/pF	12.1
$C_{\rm self\,1}$ ($C_{\rm self\,2}$)/pF	201	$C_{\rm ex1}$ ($C_{\rm ex2}$)/pF	52
$L_{11}(L_{21})/\mu$H	11.6	$L_{12}(L_{22})/\mu$H	89.6
$R_{\rm Lp}$ ($R_{\rm Ls}$)/Ω	1.05	$R_{C\rm peq}$ ($R_{C\rm seq}$)/Ω	0.26

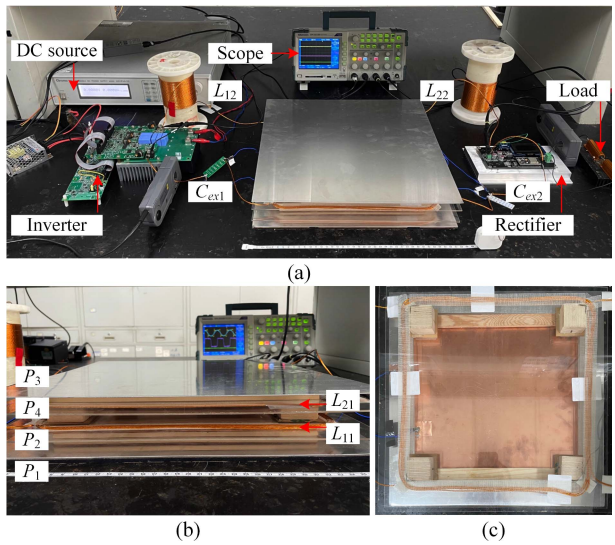

Fig. 17. Experimental prototype of the HWPT system. (a) Overview of the experimental prototype. (b) Main view of the coupler. (c) Vertical view of the coupler.

when the x-misalignment increases. As shown in Fig. 15(b), the $P_{\rm eddy}$ is not positively correlated with l_3 monotonically. With the increase of l_3, the eddy current loss decreases first and then increases.

According to the simulation results, the eddy current loss is affected by the size of coupler. Therefore, the eddy current loss can be reduced by optimizing the dimensions of coils and plates. According to [28], the eddy current loss is also affected by other factors. In general, the eddy current density is positively correlated with the frequency of the excitation source, and it is also positively correlated with the conductivity of the plates. Therefore, the eddy current loss can also be reduced by decreasing switching frequency or changing materials.

D. Electromagnetic Field Simulation

The magnetic field and electric field around the coupler are also simulated by COMSOL, and the simulation results are shown in Fig. 16. It can be seen from Fig. 16(a) that most electric flux is limited between the coupling plates without coupling misalignment. When the coupling misalignment occurs, the electric field around unaligned area increases, but it decays rapidly with the distance. Fig. 16(b) shows that the magnetic flux is constrained between outer plates without coupling misalignment. According to theoretical analysis, the coupling misalignment has little influence on the excitation current with coupling misalignment, thus the energy through inductive coupled channel decreases.

V. EXPERIMENT VERIFICATION

A. Experimental Prototype

To verify the hybrid CPT system, an experimental prototype is built up, which is shown in Fig. 17. According to the parameter design and coupler design in last section, a set of parameters can be obtained, as listed in Table III. According to the measurement data, the Q factors of the inductors and capacitors are about 620 and 2500, respectively, which is slightly smaller than the mentioned Q factors in [24]. The relative error may be caused by: 1) measurement error, 2) different size and structure of the coupler. In the experimental prototype, all reactive components are measured by HIOKI IM 3536 LCR Meter, which shows outstanding performance at a frequency below 8 MHz.

To reduce high frequency loss, the compensation inductors are made by wingding Lizi wire on PVC tubes, and the compensation capacitors are composed of multiple mica capacitors in series and parallel, as shown in Fig. 17(a). In order to improve the performance of the inverter and rectifier modules, SiC MOSFETs IMZ120R045M1 and SiC diodes GHXS030A120S are adopted in the full-bridge inverter and rectifier, respectively. The design dimensions of the hybrid coupler are illustrated in the last section, where the inductive coupler is placed between the plates of capacitive coupler, as shown in Fig. 17(b) and (c).

B. CC Performance Against Load Variation

The load-independent CC characteristic of HWPT system has been tested, as shown in Fig. 18. The waveforms of the load and inverter are recorded under different resistances. As shown in Fig. 18(a) and (b), when the load varies from 20 to 40 Ω, the input current $\boldsymbol{i_{\rm in}}$ and voltage $\boldsymbol{v_{\rm in}}$ are almost in phase. To ensure the ZVS of MOSFETs, the compensation inductors is slightly larger than the theoretical value, so $\boldsymbol{i_{\rm in}}$ is slightly lagging $\boldsymbol{v_{\rm in}}$ on the basis of ZPA. The output voltage $\boldsymbol{v_o}$ is lagging behind the input voltage $\boldsymbol{v_{\rm in}}$ by 90°, which is consistent with the theoretical analysis. The output currents of 20 and 40 Ω are 2.46 and 2.41 A, respectively.

As shown in Fig. 18(c), the peak value of the input current immediately decreases when the load resistance is switched from 40 to 20 Ω. However, the output current is almost constant at different loads, except for the switching point. At this point, the output current fluctuates slightly and reaches a new steady state

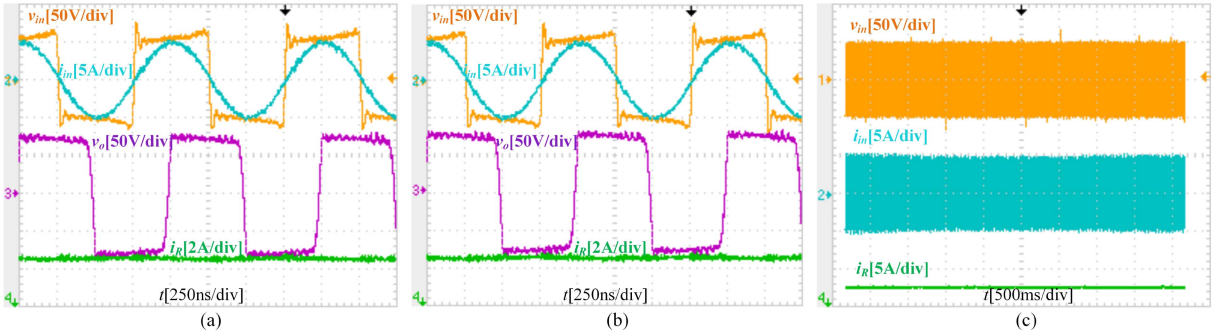

Fig. 18. Experimental waveforms of the inverter and load. (a) $R_L = 20\ \Omega$. (b) $R_L = 40\ \Omega$. (c) Dynamic process.

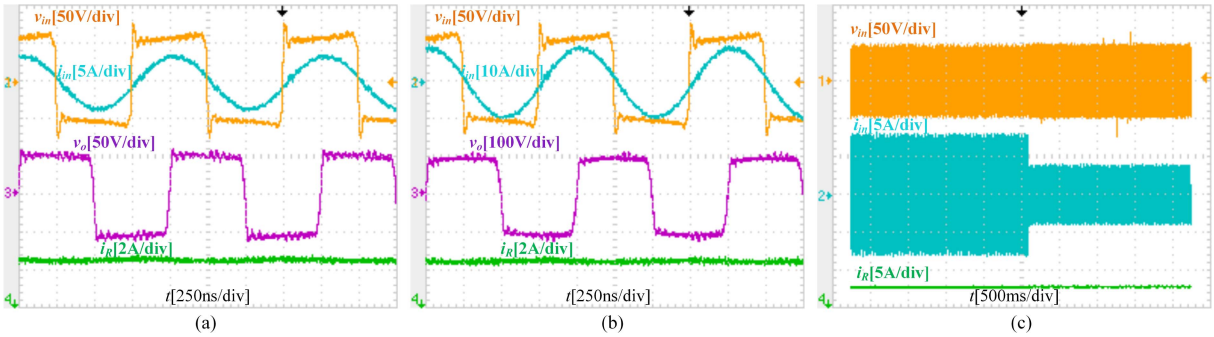

Fig. 19. Experimental waveforms of the inverter and load. (a) 0 mm misalignment. (b) 100 mm misalignment. (c) Dynamic process.

quickly. In general, Fig. 18 verifies that the output current is almost constant and in phase with the input voltage, when the load resistance changes.

C. CC Performance Against Coupling Misalignment

In addition to the load-independent CC output, the constant output current and resistive input impedance of this system are not affected by the coupling misalignment. Due to the symmetrical coupler, there is consistency on the *X*- and *Y*-axis. Fig. 19 shows the experimental waveforms at different *x*-misalignment, where the load resistance is 30 Ω. As shown in Fig. 19(a) and (b), when the coupling misalignment varies from 0 to 100 mm, the output current changes from 2.44 and 2.49 A. In similar, the input current is slightly lagging behind the input voltage under different coupling misalignments, which implies the ZVS can always be achieved. The output current is lagging behind the input current by 90°, which indicates the coupling misalignment has little effect on the resonant state. Fig. 19(c) shows the variation of the output current with the coupling misalignment. It can be seen that a virtually CC is obtained throughout the misalignment range. In general, Fig. 19 verifies that the output current is almost constant and in phase with the input voltage, when the coupling misalignment changes.

D. Comparison and Discussion

To illustrate the characteristics of the HWPT system, the CPT system with the same parameters is also tested in this article.

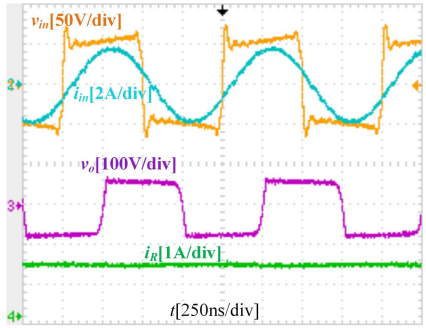

Fig. 20. Experimental waveforms of the *LC–LC* compensated CPT system.

Fig. 20 shows experimental waveforms of $\boldsymbol{v_{in}}$, $\boldsymbol{i_{in}}$, $\boldsymbol{v_o}$, and $\boldsymbol{i_{RL}}$ under full alignment at $R_L = 40\Omega$. As shown, the rms value of output current $\boldsymbol{i_{RL}}$ is 1.24 A. It can also be seen that the output voltage $\boldsymbol{v_o}$ is lagging behind the input voltage $\boldsymbol{v_{in}}$ by 90°, which is consist with the HWPT system.

According to experimental results, the output current of HWPT system is about twice as big as that of CPT system with the same coupling coefficient. With well design coupler, the HWPT can achieve the antimisalignment CC output, while the CPT and IPT systems cannot. In addition, the phase differences between the input voltage, input current, and output voltage are the same in both CPT and HWPT systems. This indicates that the output current increases and the resonant state remain unchanged with the additional inductive channel.

TABLE IV
COMPARISON OF RECENT SYSTEMS ON THIS TOPIC

literature	Method	Coupler	k_c/k	$\Delta C_M/\Delta M$	Load/Ω	CC/CV	Error
[19](CPT)	Topology	Light	∼1.00	80%	30-70	CV	8.3%
[25](CPT)	Topology	Light	∼0.20	15%	25-50	CC	–
[16](CPT)	Coupler design	Light	∼0.80	100%	–	–	–
[20](IPT)	Topology	Heavy	∼0.20	38%	16-32	CV	5.0%
[27](IPT)	Coupler design	Heavy	∼0.12	45%	20-50	CV	9.2%
[21](IPT)	Coupler design	Heavy	∼0.15	38%	20-50	CC	–
[15](HWPT)	HWPT	Light	∼0.13	30%	–	–	8.3%
This work	HWPT	Light	∼0.05	50%	20-40	CC	4.6%

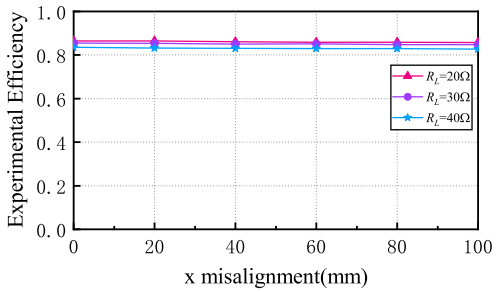

Fig. 21. Experimental efficiency at various load resistance and x-misalignments.

Fig. 21 shows the dc–dc efficiency at various load resistances and x-misalignments. It can be seen that the the system efficiency slightly decreases with the incensement of load resistance. The dc–dc reaches the maximum value at 86.5% when the load resistance is the normalized load 20 Ω. As shown, the system efficiency is approximately constant against the coupling misalignment, because the coupling misalignment does not change the reflection impedance of the HWPT system.

The method, coupler, performance, and output characteristic of recent open-loop CPT systems in this topic have been summarized in Table IV. Compared with other IPT systems, the coupler of this system is light and cheap, as well as small coupling coefficient. Compared with other CPT and HWPT systems, this work can achieve both load-independent and antimisalignment CC characteristics, as well as stable output under the same misalignment level.

VI. CONCLUSION

This article presents a novel HWPT system that maintains a constant and enhanced current output against load and coupling variations. The proposed HWPT system incorporates compensation inductors from the CPT system to create an additional inductive channel; hence, the HWPT system can be seen as the series connection of SS compensated IPT system and *LC–LC* compensated CPT system. Similar to the aforementioned two systems, the proposed HWPT system is capable of achieving load-independent current output and ZPA. With a well-designed coupler, the power transferred via the inductive channel can be compensated by the power transferred via the capacitive channel, even in the case of coupling misalignment. A 200 W experimental prototype with 20 mm transmission distance is built to validate the designed HWPT system. When the load resistance and coupling misalignment vary from 20 to 40 Ω and 0 to 100 mm x-misalignment, the HWPT system can always achieve a CC output with 4.6% variation. By setting the inductive channel, the output current of the HWPT system is twice as big as that of the CPT system.

The limitation of this study is that the system characteristics are relatively dependent on the well-designed coupler. In future research work, we will focus on improving the performance of hybrid coupler. 1) How to reduce the mutual interference between the coils and plates? 2) How to make the hybrid coupler more compact?

REFERENCES

[1] Z. Zhang, H. Pang, A. Georgiadis, and C. Cecati, "Wireless power transfer – An overview," *IEEE Trans. Ind. Electron.*, vol. 66, no. 2, pp. 1044–1058, Feb. 2019.
[2] W. Zhou, L. Huang, B. Luo, R. Mai, Z. He, and A. P. Hu, "A general mutual coupling model of MIMO capacitive coupling interface with arbitrary number of ports," *IEEE Trans. Power Electron.*, vol. 36, no. 6, pp. 6163–6167, Jun. 2021.
[3] J.-Q. Zhu et al., "A novel capacitive coupler array with free-positioning feature for mobile tablet applications," *IEEE Trans. Power Electron.*, vol. 34, no. 7, pp. 6014–6019, Jul. 2019.
[4] J. Lian and X. Qu, "An LCLC-LC-Compensated capacitive power transferred battery charger with near-unity power factor and configurable charging profile," *IEEE Trans. Ind. Appl.*, vol. 58, no. 1, pp. 1053–1060, Jan./Feb. 2022.
[5] J. Kim, K. Kim, H. Kim, D. Kim, J. Park, and S. Ahn, "An efficient modeling for underwater wireless power transfer using Z-parameters," *IEEE Trans. Electromagn. Compat.*, vol. 61, no. 6, pp. 2006–2014, Dec. 2019.
[6] R. Hasaba, K. Okamoto, S. Kawata, K. Eguchi, and Y. Koyanagi, "Magnetic resonance wireless power transfer over 10 m with multiple coils immersed in seawater," *IEEE Trans. Microw. Theory Techn.*, vol. 67, no. 11, pp. 4505–4513, Nov. 2019.
[7] B. Regensburger, S. Sinha, A. Kumar, S. Maji, and K. K. Afridi, "High-performance multi-MHz capacitive wireless power transfer system for EV charging utilizing interleaved-foil coupled inductors," *IEEE J. Emerg. Sel. Topics Power Electron.*, vol. 10, no. 1, pp. 35–51, Feb. 2022, doi: 10.1109/JESTPE.2020.3030757.
[8] V. Vu et al., "A multi-output capacitive charger for electric vehicles," in *Proc. IEEE Int. Sympo. Ind. Electron. Conf.*, 2017, pp. 565–569.
[9] L. Zhao, D. J. Thrimawithana, U. K. Madawala, A. P. Hu, and C. C. Mi, "A misalignment-tolerant series-hybrid wireless EV charging system with integrated magnetics," *IEEE Trans. Power Electron.*, vol. 34, no. 2, pp. 1276–1285, Feb. 2019.
[10] M. Zhou, F. Liu, S. Li, and X. Chen, "A 1-kW and 100-cm distance magnetically coupled resonant WPT system achieving 80% efficiency," *IEEE Trans. Transp. Electrif.*, vol. 8, no. 3, pp. 4001–4013, Sep. 2022.
[11] Y. Liu, T. Wu, and M. Fu, "Interleaved capacitive coupler for wireless power transfer," *IEEE Trans. Power Electron.*, vol. 36, no. 12, pp. 13526–13535, Dec. 2021.
[12] X. Gao et al., "Design and analysis of a new hybrid wireless power transfer system with a space-saving coupler structure," *IEEE Trans. Power Electron.*, vol. 36, no. 5, pp. 5069–5081, May 2021.

[13] D. Vincent, P. S. Huynh, and S. S. Williamson, "A link-independent hybrid inductive and capacitive wireless power transfer system for autonomous mobility," *IEEE J. Emerg. Sel. Topics Power Electron.*, vol. 3, no. 2, pp. 211–218, Apr. 2022.
[14] F. Lu, H. Zhang, H. Hofmann, and C. Mi, "An inductive and capacitive integrated coupler and its LCL compensation circuit design for wireless power transfer," in *Proc. IEEE Energy Convers. Congr. Expo.*, 2016, pp. 1–5.
[15] B. Luo, T. Long, L. Guo, R. Dai, and Z. He, "Analysis and design of inductive and capacitive hybrid wireless power transfer system for railway application," *IEEE Trans. Ind. Appl.*, vol. 56, no. 3, pp. 3034–3042, May/Jun. 2020.
[16] H. Yuan et al., "A novel anti-offset interdigital electrode capacitive coupler for mobile desktop charging," *IEEE Trans. Power Electron.*, vol. 38, no. 3, pp. 4140–4151, Mar. 2023.
[17] X. Qing, Y. Su, A. P. Hu, X. Dai, and Z. Liu, "Dual-loop control method for CPT system under coupling misalignments and load variations," *IEEE J. Emerg. Sel. Topics Power Electron.*, vol. 10, no. 4, pp. 4902–4912, Aug. 2022.
[18] C. Xia, W. Wang, G. Chen, X. Wu, S. Zhou, and Y. Sun, "Robust control for the relay ICPT system under external disturbance and parametric uncertainty," *IEEE Trans. Control Syst. Technol.*, vol. 25, no. 6, pp. 2168–2175, Nov. 2017.
[19] X. Qing, Z. Wang, Y. Su, Y. Zhao, and X. Wu, "Parameter design method with constant output voltage characteristic for bilateral LC-compensated CPT system," *IEEE J. Emerg. Sel. Topics Power Electron.*, vol. 8, no. 3, pp. 2707–2715, Sep. 2020.
[20] Y. Chen et al., "A hybrid inductive power transfer system with misalignment tolerance using quadruple-D quadrature pads," *IEEE Trans. Power Electron.*, vol. 35, no. 6, pp. 6039–6049, Jun. 2020.
[21] L. Chen, C. Zhang, T. Bo, and H. Nie, "Design and optimization of a magnetic coupling structure with high anti-offset for wireless power transfer," *J. Elect. Eng. Technol.*, vol. 18, pp. 1083–1098, 2022.
[22] Y. Wang, H. Zhang, and F. Lu, "Capacitive power transfer with series-parallel compensation for step-up voltage output," *IEEE Trans. Ind. Electron.*, vol. 69, no. 6, pp. 5604–5614, Jun. 2022.
[23] Y. Wang, H. Zhang, and F. Lu, "Current-fed capacitive power transfer with parallel-series compensation for voltage step-down," *IEEE J. Emerg. Sel. Topics Ind. Electron.*, vol. 3, no. 3, pp. 454–464, Jul. 2022.
[24] Y. Wu, Q. Chen, X. Ren, and Z. Zhang, "Efficiency optimization based parameter design method for the capacitive power transfer system," *IEEE Trans. Power Electron.*, vol. 36, no. 8, pp. 8774–8785, Aug. 2021.
[25] L. Li, Z. Wang, F. Gao, S. Wang, and J. Den, "A family of compensation topologies for capacitive power transfer converters for wireless electric vehicle charger," *Appl. Energy*, vol. 260, 2020, Art. no. 114156.
[26] J. Mai, Y. Wang, Y. Yao, and D. Xu, "Analysis and design of high-misalignment-tolerant compensation topologies with constant-current or constant-voltage output for IPT systems," *IEEE Trans. Power Electron.*, vol. 36, no. 3, pp. 2685–2695, Mar. 2021.
[27] H. Liu et al., "Anti-misalignment capability optimization for laminated magnetic couplers in wireless charging systems using balanced particle swarm optimization method," *J. Power Electron.*, vol. 23, pp. 345–354, 2023.
[28] G. Sinha and S. S. Prabhu, "Analytical model for estimation of eddy current and power loss in conducting plate and its application," *Phys. Rev. Special Topics-Accel. Beams*, vol. 14, no. 6, 2011, Art. no. 062401.
[29] X. Qing, *Performance Improvement Technology of EC-WPT System Under Variation of Coupling Capacitance and Load*. Chongqing, China: Chongqing Univ., 2021.

Xiaodong Qing (Member, IEEE) received the B.E. and Ph.D. degrees in control theory and control engineering from the School of Automation, Chongqing University, Chongqing, China, in 2015 and 2021, respectively.

He is currently a Lecturer with the School of Electrical Engineering, Chongqing University of Science and Technology, Chongqing, China. His research focuses on wireless power transfer technologies.

Zuojin Li (Member, IEEE) received the M.S. and Ph.D. degrees in automation from Chongqing University, Chongqing, China, in 2007 and 2010, respectively.

He is currently a Professor with the College of Electrical Engineering, Chongqing University of Science and Technology, Chongqing, China. He is a Lecturer with the School of Electrical Engineering, Chongqing University of Science and Technology. In 2014, he was a Postdoctor with Computing Department, UNITEC, Auckland, New Zealand. His research interests include automation control systems, image processing, pattern recognition, intelligence traffic system, and wireless power transfer technologies.

Xueying Wu received the B.E. degree in electronic information science technology and the Ph.D. degree in control theory and control engineering from Yangtze Normal University, Chongqing, China, in 2014 and 2020, respectively.

He is currently with the Chongqing University of Science and Technology, Chongqing, China. His research interests include wireless power transfer technologies, parameters optimization of capacitive power transfer systems and its control strategy.

Zhe Liu received the B.E. degree in electrical engineering from the Chongqing University of Technology, Chongqing, China, in 2014, and the M.E. degree in electrical engineering from the College of Electrical Engineering, Kunming University of Science and Technology (KUST), Kunming, China, in 2017, and the Ph.D. degree in control theory and control science from Chongqing University, Chongqing, China, in 2023.

Since 2023, he has been with the Faculty of electric power engineering with KUST, where he is currently an Special Associate Professor. His research interests include capacitive power transfer and the single capacitive coupled wireless power transfer.

Lei Zhao (Member, IEEE) received the B.S. degree from the Xi'an University of Technology, Xi'an, China, in 2011, the M.E. degree from The University of Auckland, Auckland, New Zealand, in 2013, both in electrical engineering, and the Ph.D. degree in electrical and electronic engineering from The University of Auckland, in 2019.

From 2019 to 2021, he was a Research Fellow with the Department of Electrical, Computer, and Software Engineering, The University of Auckland, with Prof. A. P. Hu. In 2022, he was with Automation School, Chongqing University, Chongqing, China, where he is currently an Associate Professor. His research interests include bidirectional hybrid inductive power transfer systems for electrical vehicle charging and high frequency power electronics.

Yugang Su (Member, IEEE) received the B.E. and M.E. degrees in industry automation and the Ph.D. degree in control theory and control engineering from Chongqing University, Chongqing, China, in 1985, 1993, and 2004, respectively.

He is currently a Professor with the School of Automation, Chongqing University. From 2008 to 2009, he was a Visiting Scholar with the University of Queensland, Brisbane, QLD, Australia. His research interests include power electronics, control theory and applications, wireless power transfer.